

RESEARCH

Open Access



Exploring the mechanism by which UCHL3 alleviates diabetic foot ulcers: FOXM1/NLRP3 inflammasome-mediated angiogenesis and endothelial cell pyroptosis

Xincheng Liao¹, Zhengying Jiang¹, Zhonghua Fu¹ and Guanghua Guo^{1*}

Abstract

Background This study investigated the role of ubiquitin C-terminal hydrolase L3 (UCHL3) in regulating endothelial cell (EC) pyroptosis and angiogenesis in diabetic foot ulcers (DFUs), with a focus on FOXM1 and NLRP3 inflammasomes.

Methods Differentially expressed genes in DFUs were identified using the GSE134431 dataset and cross-referenced with vascular formation-related factors from GeneCard and deubiquitinases from the UbiNet 2.0 database. A rat DFU model was used to evaluate wound healing, with or without UCHL3 overexpression and FOXM1 knockdown. Histological analysis and immunohistochemistry were employed to assess tissue morphology and the expression of CD31, eNOS, UCHL3, and FOXM1. In vitro, high glucose-induced human umbilical vein ECs (HUVECs) were transfected with UCHL3 overexpression and FOXM1 knockdown constructs. Cell viability, migration, and angiogenesis were assessed.

Results UCHL3 expression was significantly reduced in DFU tissues. UCHL3 overexpression promoted wound healing in a rat model, while FOXM1 knockdown impaired wound healing and vascular formation. In HUVECs, UCHL3 overexpression enhanced cell viability, migration, and angiogenesis, accompanied by reduced NLRP3 and N-GSDMD levels. FOXM1 knockdown reversed these effects, but treatment with the NLRP3 inhibitor, MCC950, alleviated this damage.

Conclusion UCHL3 enhances FOXM1 deubiquitination, inhibits NLRP3 inflammasome activation, and reduces EC pyroptosis, thereby contributing to DFU healing. UCHL3 and FOXM1 are potential therapeutic targets for DFU.

Keywords Diabetic foot ulcers, UCHL3, FOXM1, NLRP3 inflammasome, Endothelial cells

*Correspondence:

Guanghua Guo
gggg2024@126.com

¹Medical Center of Burn Plastic and Wound Repair, The First Affiliated Hospital, Jiangxi Medical College, Nanchang University, Nanchang, Jiangxi Province 330006, China



© The Author(s) 2025. **Open Access** This article is licensed under a Creative Commons Attribution-NonCommercial-NoDerivatives 4.0 International License, which permits any non-commercial use, sharing, distribution and reproduction in any medium or format, as long as you give appropriate credit to the original author(s) and the source, provide a link to the Creative Commons licence, and indicate if you modified the licensed material. You do not have permission under this licence to share adapted material derived from this article or parts of it. The images or other third party material in this article are included in the article's Creative Commons licence, unless indicated otherwise in a credit line to the material. If material is not included in the article's Creative Commons licence and your intended use is not permitted by statutory regulation or exceeds the permitted use, you will need to obtain permission directly from the copyright holder. To view a copy of this licence, visit <http://creativecommons.org/licenses/by-nc-nd/4.0/>.

Introduction

Diabetic foot ulcers (DFUs) significantly increase susceptibility to infection, elevating both the risk of amputation and post-amputation mortality rates [1, 2]. The diagnosis is mainly based on clinical manifestations, and requires comprehensive evaluation of infection signs, ulcer depth, and tissue necrosis degree [3]. The wound healing process in patients with diabetes is notably slow, and in severe cases, healing may stagnate entirely, leading to substantial psychological and physical burdens, as well as posing serious health threats [4]. In individuals with diabetes, endothelial dysfunction and compromised microcirculation severely hinder angiogenesis during wound healing [5]. Although existing treatments such as surgical intervention can promote ulcer healing, the treatment outcomes of DFU are still unsatisfactory [6, 7]. Therefore, the identification of new therapeutic targets and intervention strategies is critical for advancing DFU management.

The pathogenesis of DFUs primarily stems from chronic inflammation and inadequate angiogenesis [8]. Angiogenesis is regulated by various molecular factors and signaling pathways, with endothelial cell (EC) functions playing a pivotal role in this process [9]. However, high glucose (HG) levels render ECs highly susceptible to damage, diminishing their capacity for blood vessel formation [10]. Insufficient angiogenesis in wounds exacerbates tissue inflammation and impedes or halts wound healing [11]. Thus, mitigating HG-induced endothelial damage and enhancing angiogenic potential are critical for improving wound healing in DFU.

As a post-translational modification, ubiquitination/deubiquitination critically regulates protein stability and function, and is involved in the pathophysiology of many diseases [12]. Deubiquitinases (DUBs) counterbalance ubiquitination by removing ubiquitin moieties from target proteins, thereby modulating their function and stability [13]. Ubiquitin C-terminal hydrolase (UCH) L3 (UCHL3), a member of the UCH family of DUBs, has substrates, including Forkhead box protein M1 (FOXM1), Lactate dehydrogenase A (LDHA), and TNF receptor-associated factor 2 (TRAF2), which it deubiquitinates to modulate their activity [14]. Notably, decreased FOXM1 expression in DFU models has been associated with impaired wound healing [15], suggesting that UCHL3 may influence DFU progression through deubiquitination of FOXM1.

High-glucose environments exacerbate tissue inflammation and suppress angiogenesis in DFUs [1]. Studies have indicated that FOXM1 upregulation attenuates inflammation while promoting endothelial regeneration and vascular repair [16]. Furthermore, NACHT, LRR and PYD domains-containing protein 3 (NLRP3) inflammasome activation induces Gasdermin-D (GSDMD)

cleavage, releasing N-GSDMD, which triggers pyroptosis, a form of programmed cell death marked by inflammation [17]. Excessive cellular pyroptosis and inflammation are major impediments to wound healing in DFUs [18]. Therefore, FOXM1 may enhance DFU wound healing by suppressing NLRP3 inflammasome activation.

In this study, we hypothesized that UCHL3 binds to FOXM1 to promote its deubiquitination and potentially improve DFU outcomes. To date, there has been limited research on the role of UCHL3 in DFUs. We addressed this gap by investigating how UCHL3 modulates EC pyroptosis-mediated angiogenesis in DFUs via FOXM1 deubiquitination. Our findings underscore the critical role of UCHL3 in DFU management via the regulation of FOXM1.

Methods

Bioinformatics analysis

Gene expression data from DFUs and skin samples were obtained from the GSE134431 dataset (<https://www.ncbi.nlm.nih.gov/geo/>). Genes with significant differential expression in DFUs were screened, with the following criteria: $P < 0.01$ and $|\log\text{FoldChange}| \geq 1$. The GeneCard database (<https://www.genecards.org/>) was used to retrieve a list of angiogenesis-related genes. Using the UbiNet 2.0 database (http://ubibrowser.bio-it.cn/ubibrowser_v3/home/index), we obtained factors related to ubiquitinases (DUBs).

Rat culture and modeling

Adult male SD rats (6 weeks old, weighing 200–220 g) were purchased from Beijing Huafukang Biotechnology Co., Ltd. and housed in a pathogen-free animal room (temperature: 22–25 °C, humidity: 60–65%) with a 12 h light/dark cycle. The rats were allowed to adapt for 1 week before the experiment. The 36 rats were divided into six groups: Control, DFU, oe-NC, oe-UCHL3 (overexpressing UCHL3), oe-UCHL3 + sh-NC (overexpressing UCHL3), and oe-UCHL3 + sh-FOXM1 (overexpressing UCHL3 and FOXM1 knockdown). Type 1 diabetes mellitus was induced in all rats, except those in the control group, via a single intraperitoneal injection of streptozotocin (STZ; 100 mg/kg; S0130, Sigma-Aldrich, USA), freshly dissolved in 0.01 M sodium citrate buffer (pH 4.3). Rats were fasted for 12 h prior to injection. Control rats received an equal volume of sodium citrate buffer without STZ. After 72 h, fasting blood glucose was measured from tail vein blood. Rats with glucose levels ≥ 16.7 mmol/L were considered diabetic. To maintain a stable diabetic state and prevent severe hyperglycemia-related complications (e.g., ketoacidosis, weight loss, death), insulin (6–18 U/day; 92209ES10, Yeasen, China) was administered only to diabetic rats, not to control animals. Dosage was individually adjusted based on daily blood

glucose levels, with a target range of 16.7–33.3 mmol/L. Four weeks later, rats were anesthetized using 1.5% isoflurane (R510-22-10, Shenzhen Reward Life Science & Technology Company Limited, China), and a full-thickness, round skin wound was created on the back of the hind foot using a 5 mm disposable skin biopsy puncture device (273690, Kruse, Langeskov, Denmark) and Westcott scissors to establish a DFU model. Adenoviruses for overexpression (oe-NC, oe-UCHL3) and knockdown (sh-FOXMI 1#, 2#, and 3#) were purchased from VectorBuilder and injected subcutaneously (1×10^{11} PFU) around the wound at 0 h post-modeling. On day 14, the rats were euthanized via intravenous injection of an excessive amount of pentobarbital sodium (200 mg/kg, P3761, Sigma-Aldrich). The wound tissue was quickly removed for subsequent testing [1, 19]. Blood samples were collected via rapid heart puncture after euthanasia for further experiments. This study was approved by the Animal Ethics Committee of Hunan Evidence-Based Biotechnology Co. Ltd. (ABTZ24002).

Evaluation of the wound healing rate of rats

On days 0, 7, and 14, the wound area was recorded using a camera and analyzed using ImageJ software (National Institutes of Health, USA). Wound healing rate was calculated as follows:

$$\text{Wound healing rate} = \left[\frac{(\text{initial wound area} - \text{daily wound area})}{\text{initial wound area}} \right] \times 100\%.$$

Hematoxylin and eosin staining

Rat wound tissue was fixed in a 4% paraformaldehyde solution (158127, Sigma-Aldrich) for 24 h. After fixation, the tissue was dehydrated, made transparent, waxed, and embedded in paraffin. The tissue sections were immersed in xylene (534056P4707, Sigma-Aldrich) for 5 min to remove paraffin. Ethanol (E7023, Sigma-Aldrich) was used for hydration, and the sections were then immersed in hematoxylin staining solution (HHS16, Sigma-Aldrich) for 5 min. After differentiation in 1% hydrochloric acid alcohol, the sections were immersed in 0.2% aqueous ammonia for 1 min, returning to blue. The sections were then stained with eosin staining solution (HT110132, Sigma-Aldrich) for 1 min, dehydrated in ethanol, cleared

in xylene, and sealed with neutral gum sealing agent (HX93203, Thermo Fisher Scientific, Waltham, MA, USA). Observations were made using a Nikon Eclipse E200 microscope (Nikon Corporation, Tokyo, Japan).

Cell culture and modeling

Human umbilical vein ECs (HUVECs; C2519A, Lonza, Basel, Switzerland) were purchased and inoculated into EGM-2 medium (CC-3162, Lonza) containing 10% FBS under moist conditions at 37 °C and 5% CO₂. HUVECs were cultured in EGM-2 medium at 50–70% confluence and transfected with 2 µg of either oe-NC (empty vector control) or oe-UCHL3 plasmid using Lipofectamine 3000 (Thermo Fisher) for 24 h, followed by 48 h culture in fresh medium. Finally, UCHL3 and FOXM1 expression in HUVECs was verified by Western blotting (WB). In normal DMEM (5 mM glucose, D6046, Sigma-Aldrich), 25 mM glucose was added to prepare a high-glucose medium (30 mM). The cells were incubated with normal DMEM and high-glucose DMEM for 24 h, followed by subsequent measurements [20, 21].

Cell Counting Kit-8

Cell viability was determined using a Cell Counting Kit-8 (CCK-8) assay kit (C0037; Beyotime, Shanghai, China). Cells (3×10^3 /well) were inoculated onto a 96-well plate. After washing the cells with PBS, they were cultured at 37 °C for 2 h in 10 µL CCK-8 and 90 µL serum-free medium, with 95% air and 5% CO₂. The OD was measured at 450 nm using a microplate reader (BioTek Instruments Inc., Winooski, Vermont, USA) to evaluate cell viability.

RT-qPCR

Total RNA was extracted using TRIzol reagent (R1030, Prilai, Beijing, China). The extracted RNA was quantified using an HD-UV90 spectrophotometer (Shandong Hold Electronic Technology Co., Weifang, China) according to the manufacturer's instructions. Two micrograms of RNA underwent reverse transcription using the Vazyme DLR102 SynScript® III One-Step RT Kit (DLR102, Vazyme Biotech Co., Ltd., Nanjing, China) to create cDNA. A thermal cycler (Applied Biosystems, California, USA) was used to conduct the RT-qPCR. The relative expression level was calculated using the $2^{-\Delta\Delta Ct}$ method [22]. *GAPDH* was used as the internal control. The primer sequences are shown in Table 1.

Western blotting

The cells were added to radioimmunoprecipitation assay solution (89900, Thermo Fisher Scientific) and lysed on ice for 30 min with shaking every 5 min. Centrifugation was performed at 12,000 rpm for 10 min at 4 °C to collect the supernatant. The protein concentration of each

Table 1 The primer sequences for RT-qPCR

Gene	Primer sequences (5'-3')	
UCHL3	Forward	CAAACAATCAGCAATGCCTGTGG
	Reverse	GGCTCATTGACACAGATTCCTCC
GAPDH	Forward	GTCTCCTCTGACTTCAACAGCG
	Reverse	ACCACCTGTTGCTGTAGCCAA

sample was measured using a BCA protein detection kit (23227; Thermo Fisher Scientific). After SDS-PAGE gel electrophoresis, the protein was transferred to a PVDF membrane (88518, Thermo Fisher Scientific), and the membrane was sealed with 5% skimmed milk powder for 1 h following electroporation. Anti-TSP-1 antibody (1:2000, HY-P83750, MedChemExpress, New Jersey, USA), Anti-UCHL3 antibody (1:1000, A0280, Abclonal, Düsseldorf, Germany), Anti-UCHL3 antibody (1:10,000, ab126621, Abcam, Cambridge, Massachusetts, USA), anti-FOXM1 antibody (1:1000, ab180710, Abcam), anti-NLRP3 antibody (1:1000, 30109-1-AP, Santa Cruz Biotechnology, Inc., Shanghai, China), anti-cleaved N-terminal GSDMD antibody (1:1000, ab215203), UB (1:60,000, 80992-1-RR, Proteintech Group, Wuhan, China), and anti-GAPDH antibody (1:5000, 4A9L6, Thermo Fisher Scientific) were added to the membranes and incubated overnight at 4 °C. Rat anti-rabbit IgG horseradish peroxidase (HRP) antibody was diluted in 5% skim milk (1:20,000, 31464, Thermo Fisher Scientific) and incubated at room temperature for 1 h. Finally, the protein bands were developed using an ECL luminescent reagent (32106, Thermo Fisher Scientific) and analyzed for optical density using ImageJ image analysis software.

Immunohistochemistry

Rat wound tissue slices were placed in sodium citrate buffer (C9999; Sigma-Aldrich) for antigen repair. Sections were incubated with a blocking solution containing 5% bovine serum albumin (A9647, Sigma-Aldrich) at room temperature for 30–60 min. The sections were then incubated overnight at 4 °C with anti-CD31 antibody (1:4000, 11265-1-AP, Proteintech Group), anti-eNOS antibody (1:500, 27120-1-AP, Proteintech Group), FOXM1 antibody (10 µg/mL, AA 209–460, Antibodies Online, Pennsylvania, USA), and UCHL3 antibody (1:50, MA5-44997, Thermo Fisher Scientific). The sections were incubated with HRP secondary antibody (1:1000, 31470, Thermo Fisher Scientific) at room temperature for 30 min. The sections were then incubated with DAB colorimetric reagent (SK-4100; Vector Laboratories, Burlingame, CA, USA), counterstained with hematoxylin, dehydrated, and sealed with neutral gum. Protein expression levels were quantitatively analyzed using ImageJ image analysis software by observing and capturing the staining results under a microscope.

Immunoprecipitation

The cells were collected and lysed using a lysis buffer containing protease inhibitors and placed on ice for 30 min. The cell debris was removed by high-speed centrifugation, and the supernatant was collected. UCHL3 antibody (PA5-81106, Thermo Fisher Scientific) and IgG antibody (SAB5600195, Sigma-Aldrich) were added, and

the mixture was incubated overnight at 4 °C. Protein A/G beads (88802, Thermo Fisher Scientific) were added and incubated for 2 h to allow the antibody-antigen complex to bind to the beads. The beads were washed three times and centrifuged to remove the supernatant. Sample buffer was added, and the samples were boiled for 5 min for Western blot analysis.

Deubiquitination analysis

HUVECs were cultured to a confluence of 70–80%, after which Lipofectamine™ 3000 transfection reagent (L30000008, Thermo Fisher Scientific) and sh-NC or sh-UCHL3 plasmids were added to the culture dish and incubated for 6 h. The medium was then replaced, and the cells were treated with 10 µM proteasome inhibitor MG132. After 48 h of transfection, the cells were collected and immunoprecipitated with FOXM1 antibody (PA5-27631, Thermo Fisher Scientific). Ub and FOXM1 expression were detected by WB.

Cycloheximide (CHX) detection

First, a suitable cell line was selected for routine culture, and the cells were divided into control and experimental groups. In the experimental group, UCHL3 was knocked down. Fifty micrograms per milliliter of CHX (C7698, Sigma Aldrich) was added to the experimental and control group cells, and the cells were collected at different time points (0, 0.5, 1, 2 h). WB was performed to analyze the effect of UCHL3 on FOXM1 protein stability.

Scratch test

ECs were cultured in culture dishes until they formed a dense monolayer. A sterile pipette tip (200 µL) was then used to scratch a single layer of cells, simulating a wound, and creating a “blank” area in the cell layer. Subsequently, the crossed cells were removed and replaced with serum-free EGM-2 medium (CC-3162; Lonza, Basel, Switzerland) to ensure that no floating cells reattached to the scratched area. The culture dish was returned to the incubator, and the scratched area was observed and photographed at 0 and 24 h using a microscope to observe and record cell migration. The width changes of the scratch areas at different time points were measured and compared using ImageJ image analysis software to evaluate the speed of cell migration.

Tube formation experiment

Matrigel (356231, Corning, New York, USA) was added to a 96-well plate, and the plate was incubated in a 37 °C incubator for 30 min to solidify the matrix gel. The prepared ECs were evenly inoculated onto the solidified matrix gels. Subsequently, the 96-well plate was placed in an incubator and incubated for 6 h at 37 °C and 5% CO₂ conditions. Images were captured after 6 h using

an inverted microscope (Nikon, Tokyo, Japan). ImageJ image analysis software was used to analyze the captured images and measure and quantify the total length of the tubular structure to evaluate the angiogenic ability of the ECs.

Statistical analysis

Statistical analysis was performed using Prism 9 software (GraphPad, USA), and the data were expressed as mean \pm SD. Differences between the two groups were analyzed using a t-test. For three or more sets of data, one-way or two-way ANOVA was used, and Tukey's test was applied for post-hoc testing. Statistical significance was set at $P < 0.05$, indicating a statistically significant difference.

Results

UCHL3 is lowly expressed in DFU

To identify differentially expressed genes in DFUs, we compared DFU samples with diabetic skin samples from the GSE134431 dataset, using thresholds of $P < 0.01$ and $|\log_{2}FC| \geq 1$ (Fig. 1A). An intersection analysis was conducted with angiogenesis-related factors from GeneCard and DUB factors from the UbiNet 2.0 database, resulting in three overlapping factors: *UCHL3*, *PSMD14*, and *TNFAIP3* (Fig. 1B). *UCHL3* showed the smallest p-value in the dataset. To investigate the function of *UCHL3* in DFU, we developed a rat model. We found that blood glucose levels significantly increased after modeling (DFU pathological rat model, Fig. 1C). Evaluation of the wound healing rate demonstrated a significant reduction in healing after modeling (Fig. 1D). Hematoxylin and eosin staining revealed that the formation of new blood vessels was markedly reduced in the DFU model (Fig. 1E). CD31 and eNOS, both critical for angiogenesis and vascular function [23, 24], showed decreased expression in DFU wound tissues as confirmed by immunohistochemistry, along with reduced *UCHL3* expression (Fig. 1G, H). In addition, WB detection found that the expression of VEGF, a marker of angiogenesis, was significantly decreased and the expression of TSP-1 was significantly increased in the wound tissue of rats after modeling (Fig. 1I). These results indicate that the DFU rat model was successfully established and that *UCHL3* was downregulated in DFU rats.

Overexpression of UCHL3 alleviates DFU

To assess the therapeutic potential of *UCHL3*, we evaluated its effects on DFU. The results indicated that *UCHL3* expression was significantly elevated in the oe-*UCHL3* group compared to the oe-NC group (Fig. 2A). Moreover, after the upregulation of *UCHL3*, blood glucose levels in DFU rats significantly decreased (Fig. 2B). The wound healing rate analysis demonstrated

a marked improvement with *UCHL3* overexpression, showing a significantly accelerated healing rate (Fig. 2C). Histological analysis revealed a notable increase in newly developed blood vessels in the wound tissue of *UCHL3*-overexpressing rats (Fig. 2D). Additionally, immunohistochemical analysis showed that *UCHL3* overexpression led to increased expression of CD31 and eNOS in the wound tissue (Fig. 2E-F). WB assay showed that the upregulation of *UCHL3* significantly promoted the expression of VEGF and inhibited the expression of TSP-1 in the wound tissue of DFU rats (Fig. 2G). These findings suggest that *UCHL3* overexpression effectively alleviates DFU, likely through mechanisms involving enhanced angiogenesis.

UCHL3 inhibits EC damage and promotes angiogenesis

To elucidate the role of *UCHL3* in endothelial function, we examined HG-induced damage in HUVECs with *UCHL3* overexpression. *UCHL3* expression was quantified using RT-qPCR and WB, demonstrating a marked reduction following HG exposure, whereas *UCHL3* overexpression significantly elevated its expression levels under these conditions (Fig. 3A, B). Cell viability analysis using the CCK-8 assay indicated a significant decrease in the HG group relative to the normal glucose (NG) group. Notably, *UCHL3* overexpression significantly enhanced cell viability in the HG + oe-*UCHL3* group compared to that in the HG + oe-NC group (Fig. 3C). Furthermore, the scratch assay revealed a significant reduction in HUVEC migration under HG conditions, which was notably improved by *UCHL3* overexpression (Fig. 3D). Tube formation assays indicated that *UCHL3* overexpression effectively counteracted the HG-induced suppression of the angiogenic capacity of HUVECs (Fig. 3E). These findings suggest that *UCHL3* plays a protective role against HG-induced EC damage while enhancing angiogenic potential, underscoring its therapeutic potential in vascular complications associated with diabetes.

UCHL3 binds to FOXM1 and promotes FOXM1 deubiquitination while inhibiting NLRP3 inflammasome activation

Using Ubibrowser 2.0, we analyzed the downstream targets of *UCHL3* (Fig. 4A). Previous studies have indicated that FOXM1 plays a critical role in promoting wound healing in DFUs [25]. Our experimental validation demonstrated that HG exposure resulted in decreased FOXM1 expression in HUVECs; however, cells overexpressing *UCHL3* exhibited increased FOXM1 levels compared to control cells (Fig. 4B). To further investigate the interaction between *UCHL3* and FOXM1, immunoprecipitation assays were performed. The results indicated a significant enrichment of FOXM1 in association with *UCHL3* compared to that in the control IgG group,

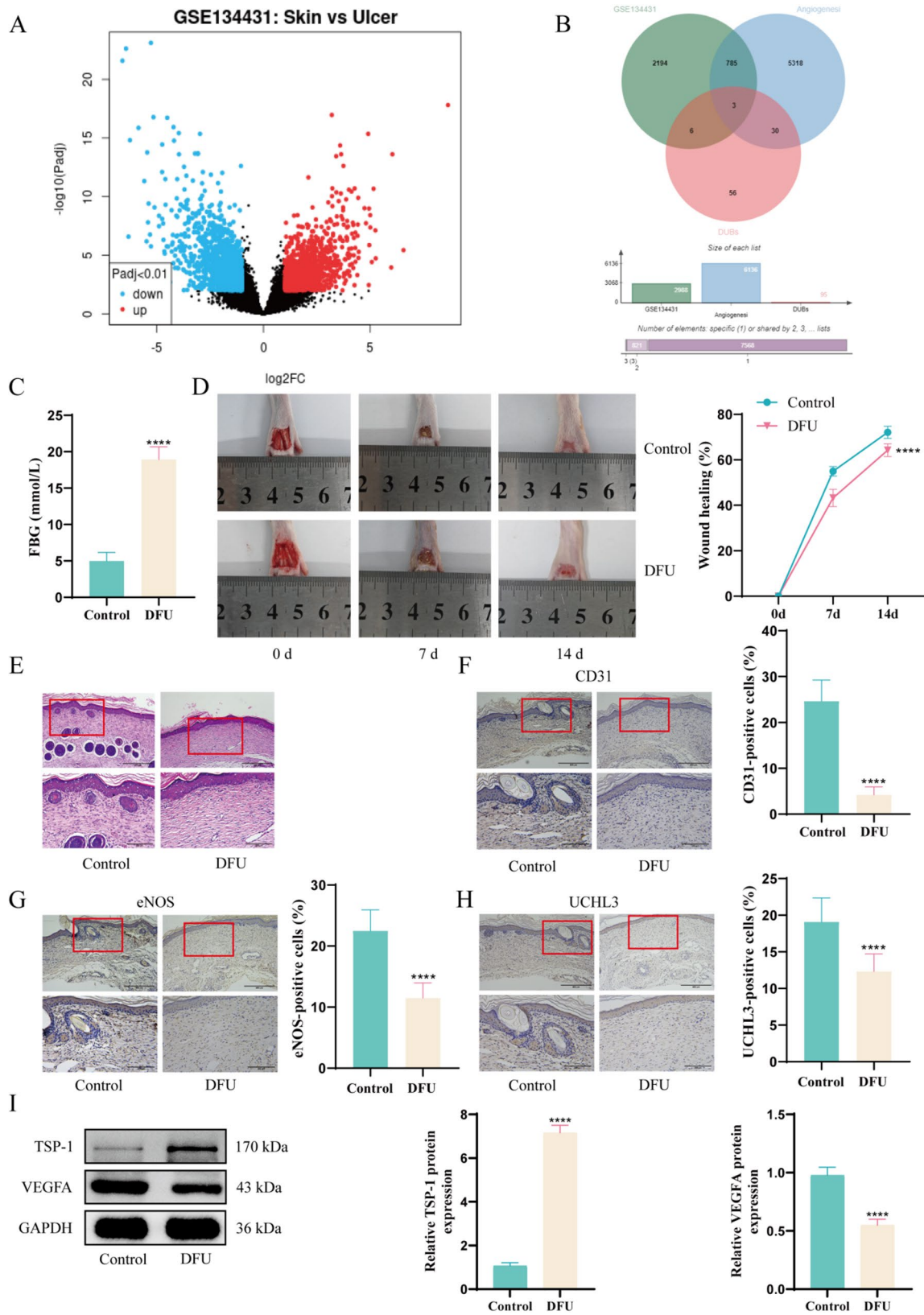


Fig. 1 (See legend on next page.)

(See figure on previous page.)

Fig. 1 UCHL3 is lowly expressed in DFU. **(A)** Volcanic map of differentially expressed genes in GSE134431. **(B)** The intersection Venn diagram of DEGs with vascular formation related factors downloaded from GeneCard database and DUBs collected from UbiNet 2.0 database. **(C)** Detection of changes in blood glucose levels in rats before and after modeling. **(D)** Assessment of alterations in wound healing rate in rats before and after modeling. **(E)** HE staining was used to compare histological and morphological characteristics of the wound before and after modeling. **(F)** Immunohistochemical analysis of changes in CD31 expression in wound tissue before and after modeling. **(G)** Immunohistochemical analysis of changes in eNOS expression in wound tissue before and after modeling. **(H)** Immunohistochemical analysis of changes in UCHL3 expression in wound tissue before and after modeling. **(I)** WB detection of changes in angiogenesis-related proteins (VEGF and TSP-1) in rat wound tissues before and after modeling. $n=6$. The magnification of images **D**, **E**, **F** and **G** is 100 times (scale = 400 μm) and 200 times (scale = 200 μm) respectively. **** $P < 0.0001$. The detection between the two groups was analyzed using t-test. Two factor analysis of variance (ANOVA) will be used for three or more sets of data, and Tukey's will be used for post hoc testing

confirming the binding relationship between these two proteins (Fig. 4C). We also assessed the effect of UCHL3 knockdown on FOXM1 ubiquitination after treatment with MG132. The findings revealed that UCHL3 knockdown enhanced the interaction between ubiquitin and FOXM1, suggesting that UCHL3 facilitates the deubiquitination of FOXM1 (Fig. 4D). Moreover, CHX treatment indicated that the knockdown of UCHL3 significantly decreased FOXM1 stability (Fig. 4E). The NLRP3 inflammasome promotes cellular pyroptosis [26, 27]. In our study, HG exposure resulted in elevated expression of NLRP3 and N-GSDMD in HUVECs; conversely, UCHL3 overexpression mitigated these increases (Fig. 4F). Collectively, these results suggest that UCHL3 interacts with FOXM1 to promote its deubiquitination, while concurrently inhibiting the activation of the NLRP3 inflammasome, highlighting a critical molecular mechanism underlying EC protection in the context of diabetes-related complications.

Knockdown of FOXM1 leads to pyroptosis of ECs and inhibits angiogenesis

To investigate the effects of FOXM1 knockdown in ECs overexpressing UCHL3, we performed western blot analysis. The results indicated that FOXM1 expression was significantly reduced in the oe-UCHL3 + sh-FOXM1 group compared to that in the oe-UCHL3 + sh-NC group, whereas the expression levels of NLRP3 and N-GSDMD were significantly elevated (Fig. 5A). In order to further clarify the regulatory mechanism of uchl3-foxm1 axis in DFU, DMSO was used as control, and mcc950 (10 μm), a specific inhibitor of NLRP3 inflammasome, was used for intervention in this study. HG-induced FOXM1 knockdown in ECs overexpressing UCHL3 markedly reduced cell viability. However, the addition of the NLRP3 inhibitor MCC950 partially mitigated the decrease in cell activity caused by FOXM1 knockdown (Fig. 5B). In scratch assays, ECs overexpressing UCHL3 exhibited a significant decline in migration rate following FOXM1 knockdown. Notably, the introduction of MCC950 into these cells significantly enhanced their migration rate, even after FOXM1 knockdown (Fig. 5C). Furthermore, tube formation assays revealed that FOXM1 knockdown in ECs overexpressing UCHL3 significantly reduced the length of the angiogenic structures (Fig. 5D). These findings

indicated that FOXM1 knockdown promotes pyroptosis in ECs and impairs angiogenesis, highlighting the critical role of FOXM1 in maintaining EC viability and function during UCHL3 overexpression.

UCHL3 alleviates DFU by promoting the expression of FOXM1

We constructed a DFU rat model with UCHL3 overexpression to investigate the role of FOXM1 in wound healing. Immunohistochemical analysis revealed that FOXM1 expression was significantly reduced in the oe-UCHL3 + sh-FOXM1 group compared to the oe-UCHL3 + sh-NC group (Fig. 6A). After the downregulation of FOXM1, the blood glucose levels in rats were significantly reduced (Fig. 6B). Furthermore, FOXM1 knockdown in model rats markedly decreased the wound healing rate (Fig. 6C). Additionally, there was a significant reduction in the formation of new blood vessels and mature granulation tissue (Fig. 6D). Immunohistochemical assessments demonstrated that the inhibition of FOXM1 expression in model rats led to a substantial decrease in the expression levels of CD31 and eNOS, both of which are critical markers of angiogenesis (Fig. 6E, F). WB analysis found that downregulation of FOXM1 significantly reversed the upregulation of UCHL3 on VEGF expression promotion and inhibition of TSP-1 expression (Fig. 6G). In summary, these results indicate that the knockdown of FOXM1 inhibits the beneficial effects of UCHL3 on DFU, underscoring the importance of FOXM1 in mediating the therapeutic actions of UCHL3 in this model of diabetes-related complications.

Discussion

DFUs are a significant and prevalent complication of diabetes that profoundly impact patients' quality of life, primarily due to the associated risk of amputation [28]. This complication is largely attributed to impaired neovascularization induced by HG levels, leading to ischemia, hypoxia, and difficulties in transporting essential nutrients to damaged tissues [29]. Chronic wounds not only diminish patients' quality of life but also contribute to an increased mortality rate [30]. Although the current treatment modalities for DFU are comprehensive, substantial challenges remain, resulting in suboptimal

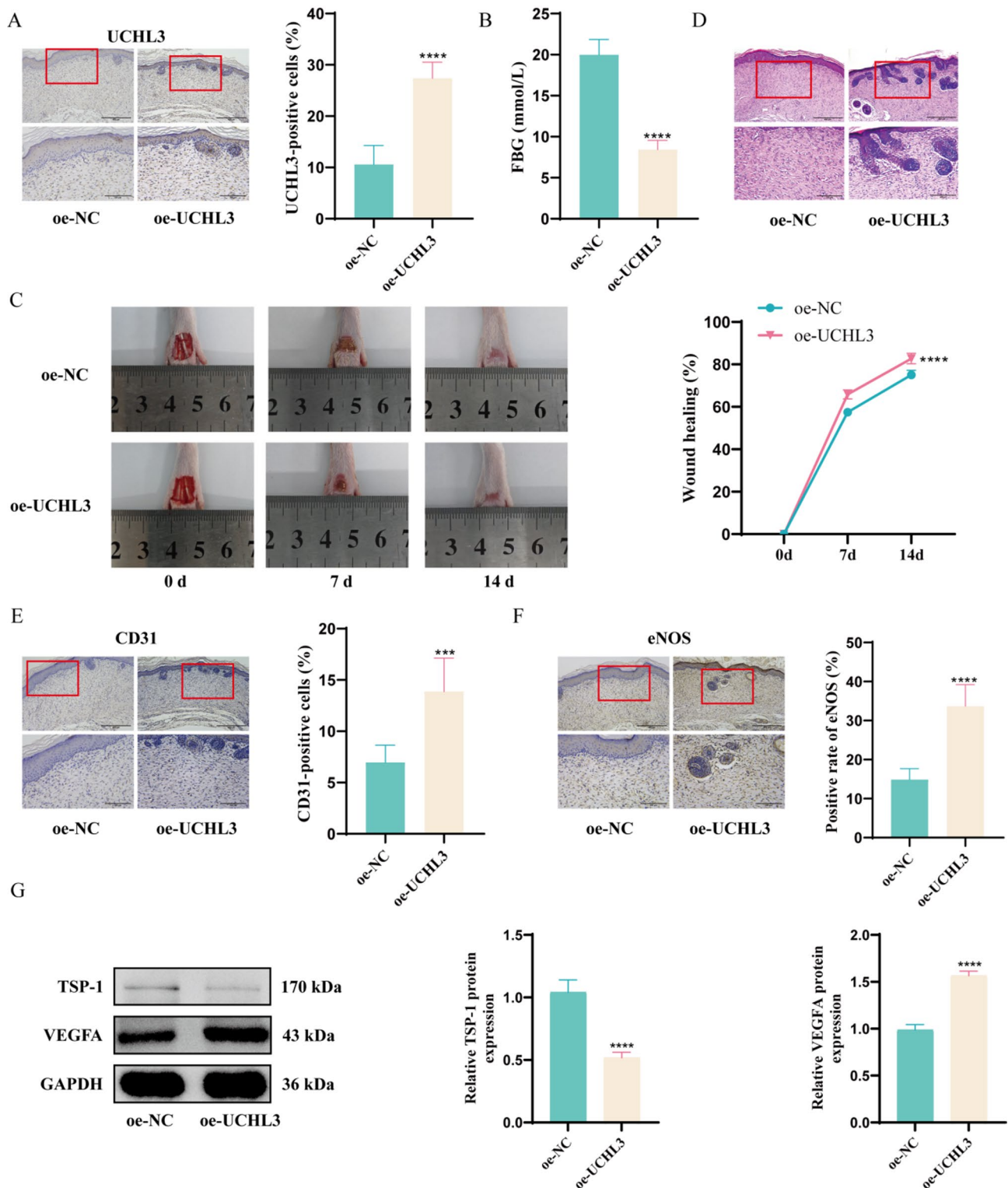


Fig. 2 Overexpression of UCHL3 alleviates DFU. **(A)** Immunohistochemical detection of UCHL3 expression to verify overexpression efficiency. **(B)** Assessment of wound healing rate in rats after UCHL3 overexpression. **(C)** Detection of blood glucose levels in rats to evaluate metabolic effects of UCHL3 overexpression. **(D)** HE staining was used to analyze histological and morphological changes in the wound after UCHL3 overexpression. **(E)** Immunohistochemical detection of CD31 expression to assess angiogenesis following UCHL3 overexpression. **(F)** Immunohistochemical detection of eNOS expression to evaluate endothelial function after UCHL3 overexpression. **(G)** WB analysis of angiogenesis-related proteins (VEGF and TSP-1) in wound tissues after UCHL3 overexpression. $n=6$. The magnification of images **A**, **D**, **E** and **F** is 100 times (scale=400 μm) and 200 times (scale=200 μm) respectively. *** $P < 0.001$, **** $P < 0.0001$. The detection between the two groups was analyzed using t-test. Two factor analysis of variance (ANOVA) will be used for three or more sets of data, and Tukey's will be used for post hoc testing

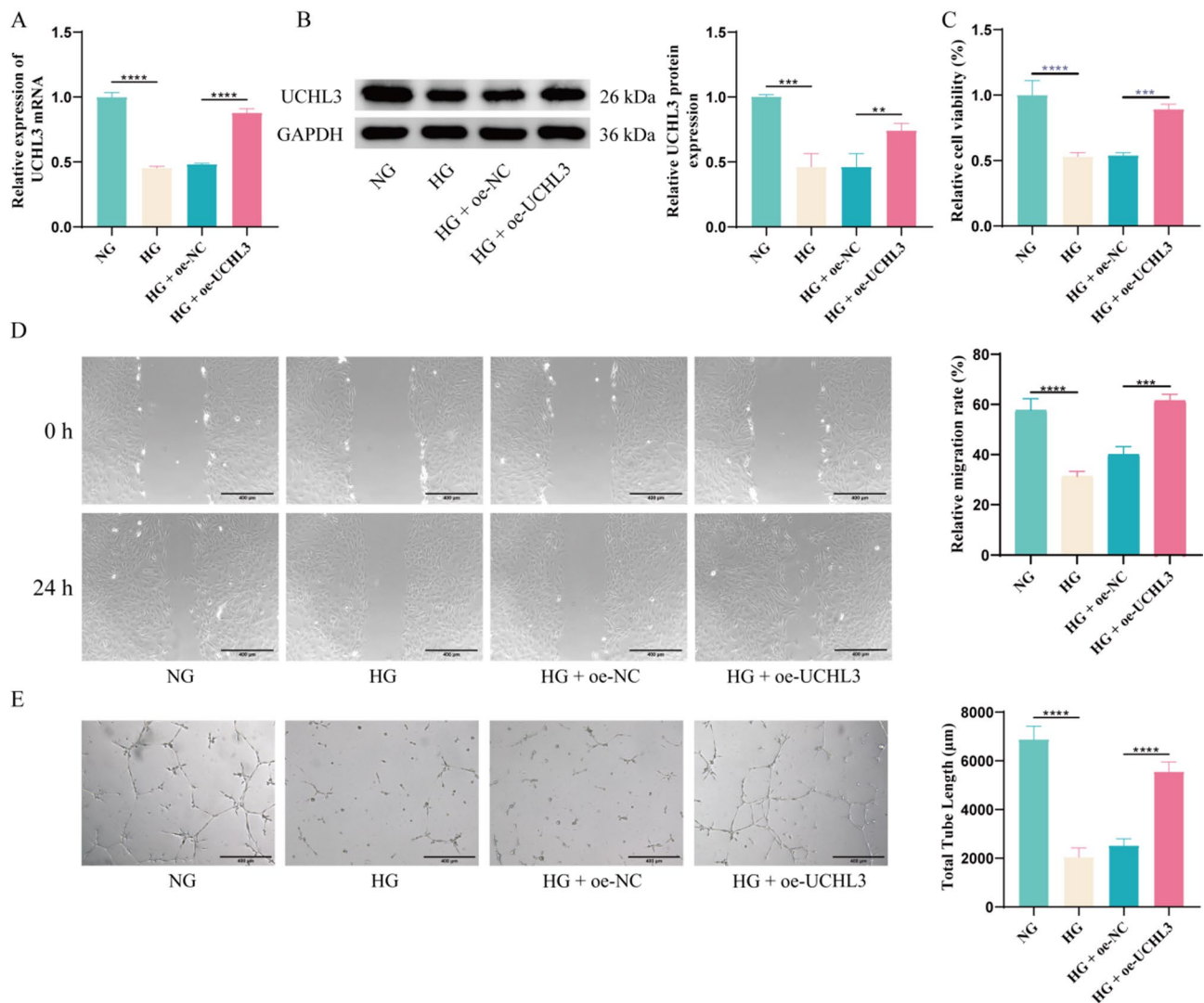


Fig. 3 UCHL3 inhibits endothelial cell damage and promotes angiogenesis. **(A)** RT-qPCR detection of *UCHL3* mRNA expression levels in HUVECs. **(B)** WB detection of UCHL3 protein expression in HUVECs. **(C)** CCK-8 assay to measure HUVEC proliferation activity. **(D)** Scratch wound healing assay to evaluate HUVEC migration ability. **(E)** Tube formation assay to assess angiogenesis capacity of HUVECs. $n=3$. The magnification of images **D** and **E** is 100 times (scale=400 μm). ** $P < 0.01$, *** $P < 0.001$, **** $P < 0.0001$. Three or more sets of data were analyzed using one-way ANOVA and subjected to post hoc testing using Tukey's

therapeutic outcomes in many patients [31]. The TRIM family has been reported to be associated with inflammation and angiogenesis in endothelial cells ECs [32, 33]. Using bioinformatics analysis, we identified three deubiquitinating factors associated with diabetic nephropathy: UCHL3, PSMD14, and TNFAIP3. UCHL3 plays an important role in regulating protein deubiquitination, contributing to the maintenance of intracellular protein homeostasis and regulation of various cellular processes [14]. PSMD14, a component of the 26 S proteasome, participates in deubiquitination by

regulating protein degradation and cell cycle control [34]. TNFAIP3 inhibits the NF- κ B signaling pathway through its deubiquitination activity and exerts immunomodulatory and anti-inflammatory effects [35]. In our dataset, UCHL3 showed the highest statistical significance, suggesting that it might play a key role in the biological processes or pathological mechanisms under investigation. In our study, we observed a significant downregulation of UCHL3 in both DFU rat models and HG-treated ECs, suggesting that UCHL3 may play a crucial role in the pathophysiology of DFU.

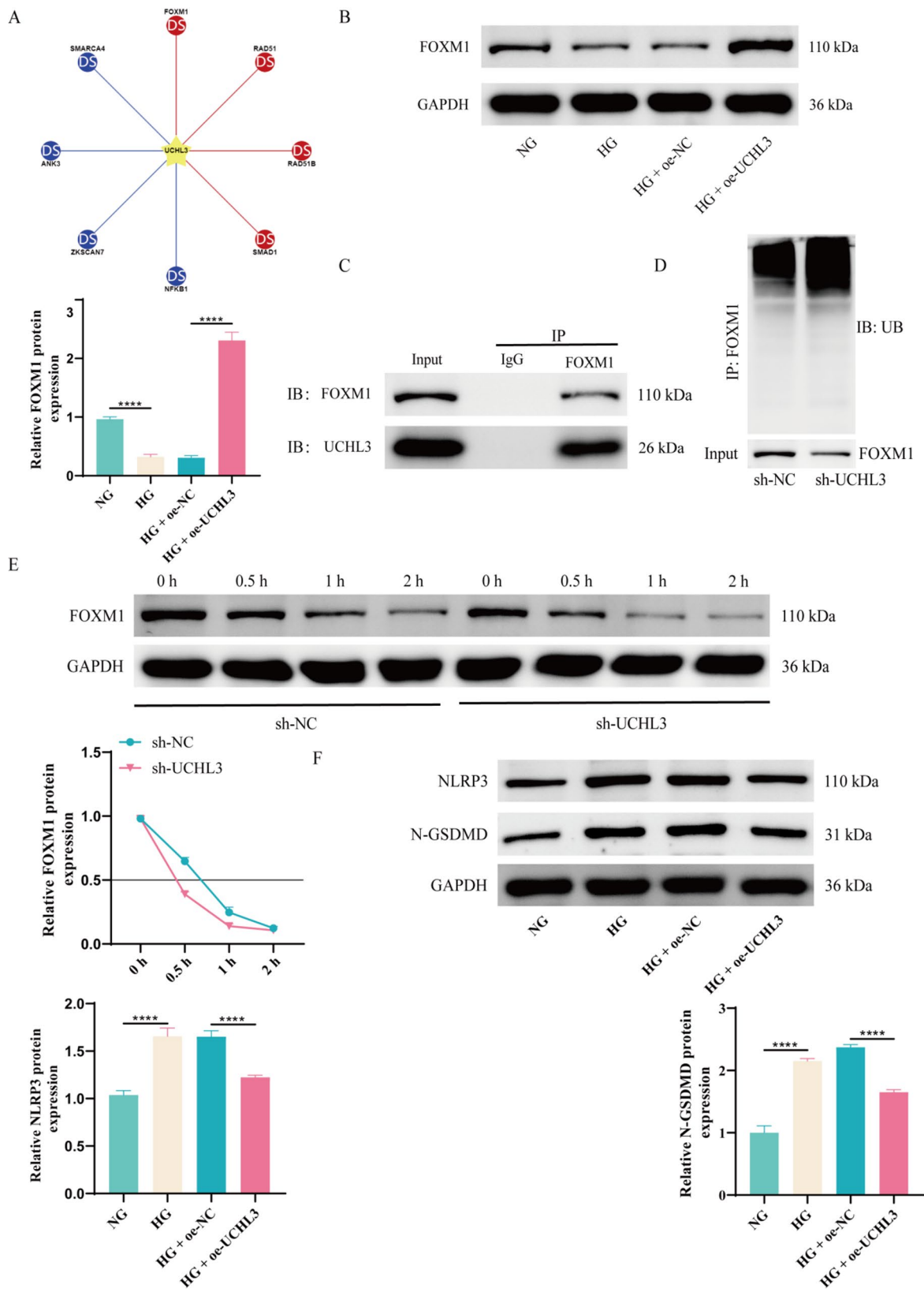


Fig. 4 (See legend on next page.)

(See figure on previous page.)

Fig. 4 UCHL3 binds to FOXM1 and promotes FOXM1 deubiquitination while inhibiting NLRP3 inflammasome activation. **(A)** The targeting relationship of UCHL3 in Ubibrowser 2.0. **(B)** WB analysis of FOXM1 expression in HUVECs. **(C)** Immunoprecipitation detection of the binding relationship between UCHL3 and FOXM1. **(D)** Immunoprecipitation assay was used to detect the deubiquitination modification of FOXM1 by UCHL3. **(E)** CHX treatment was used to detect the effect of UCHL3 on the stability of FOXM1 protein. **(F)** WB detection of NLRP3 and N-GSDMD in HUVECs. $n = 3$. **** $P < 0.0001$. Three or more sets of data will be analyzed using one-way or two-way ANOVA, and Tukey's will be used for post hoc testing

The generation of new blood vessels is crucial in the wound healing process in patients with DFU, as hypoxia in the wound tissue caused by vascular injury can delay healing [36]. In normal wound healing, angiogenesis relies on a delicate balance between promoting vascular growth and proliferation and supporting vascular maturation and stasis [11]. However, in patients with diabetes, this balance is disrupted, severely hindering angiogenesis and leading to slow or non-healing wounds [37]. Our experiments demonstrated that HG conditions damaged HUVECs with decreased cell activity, impaired migration, and reduced angiogenic capacity. Furthermore, we observed a decrease in the number of newly developed blood vessels in the DFU rat model, which was detrimental to angiogenesis and wound healing in patients with diabetes. By validating the role of UCHL3 through overexpression, we confirmed that its overexpression significantly ameliorated these adverse effects. This suggests that promoting wound healing in patients with DFU through UCHL3 may be an effective therapeutic strategy.

FOXM1 is a transcription factor associated with cell proliferation and is widely expressed during the cell cycle [38]. Our findings indicate that HG treatment of HUVECs resulted in increased FOXM1 expression in cells overexpressing UCHL3. In addition, we demonstrated that UCHL3 promotes the deubiquitination of FOXM1. Ubiquitination of FOXM1 promotes protein degradation, whereas UCHL3 enhances FOXM1 protein stability by promoting deubiquitination. We also found that the alleviating effect of UCHL3 on DFU was reversed by inhibiting FOXM1 expression. Previous studies have shown that FOXM1 promotes endothelial regeneration and vascular repair in lung tissue while alleviating inflammation [16]. Notably, downregulation of FOXM1 expression in DFU mice has been linked to impaired wound healing [15]. These observations suggest that FOXM1 facilitates endothelial regeneration and vascular repair in DFU by suppressing inflammatory responses.

Additionally, activation of the NLRP3 inflammasome has been associated with inflammation and pyroptosis [27]. Our results indicate that NLRP3 expression levels were reduced in cells overexpressing UCHL3. However, inhibition of FOXM1 expression increased NLRP3 and N-GSDMD expression levels. GSDMD mediates pro-inflammatory cell lysis, leading to pyroptosis. The NLRP3 inflammasome can induce GSDMD lysis, resulting in the release of N-GSDMD, which drives pyroptotic cell death [17]. In our experiments, we induced HG levels in HUVECs overexpressing UCHL3 by knocking down FOXM1 and using NLRP3 inhibitors. Under these conditions, we observed a decrease in FOXM1 expression and an increase in NLRP3 and N-GSDMD expression along with the inhibition of cell viability and angiogenesis. However, the addition of MCC950 reversed these adverse effects. These findings support our hypothesis that UCHL3 inhibits NLRP3 inflammasome activation and pyroptosis via FOXM1 deubiquitination, thereby promoting wound healing in DFU rats.

Although this study demonstrated that UCHL3 promotes wound healing by mediating the deubiquitination of FOXM1 in a DFU rat model and high glucose-induced endothelial cells, we recognize that UCHL3, as a deubiquitinating enzyme, may regulate multiple substrates that collectively contribute to the wound healing process. Therefore, in future studies, we plan to employ high-throughput approaches such as proteomic screening to systematically identify additional potential substrates of UCHL3, in order to gain a more comprehensive understanding of its regulatory network and biological functions. Moreover, considering the important roles of keratinocytes and fibroblasts in tissue repair, we also intend to incorporate these cell types in subsequent experiments to further investigate the role of UCHL3 in intercellular interactions, thereby elucidating the multicellular mechanisms underlying diabetic wound healing in a more integrated manner.

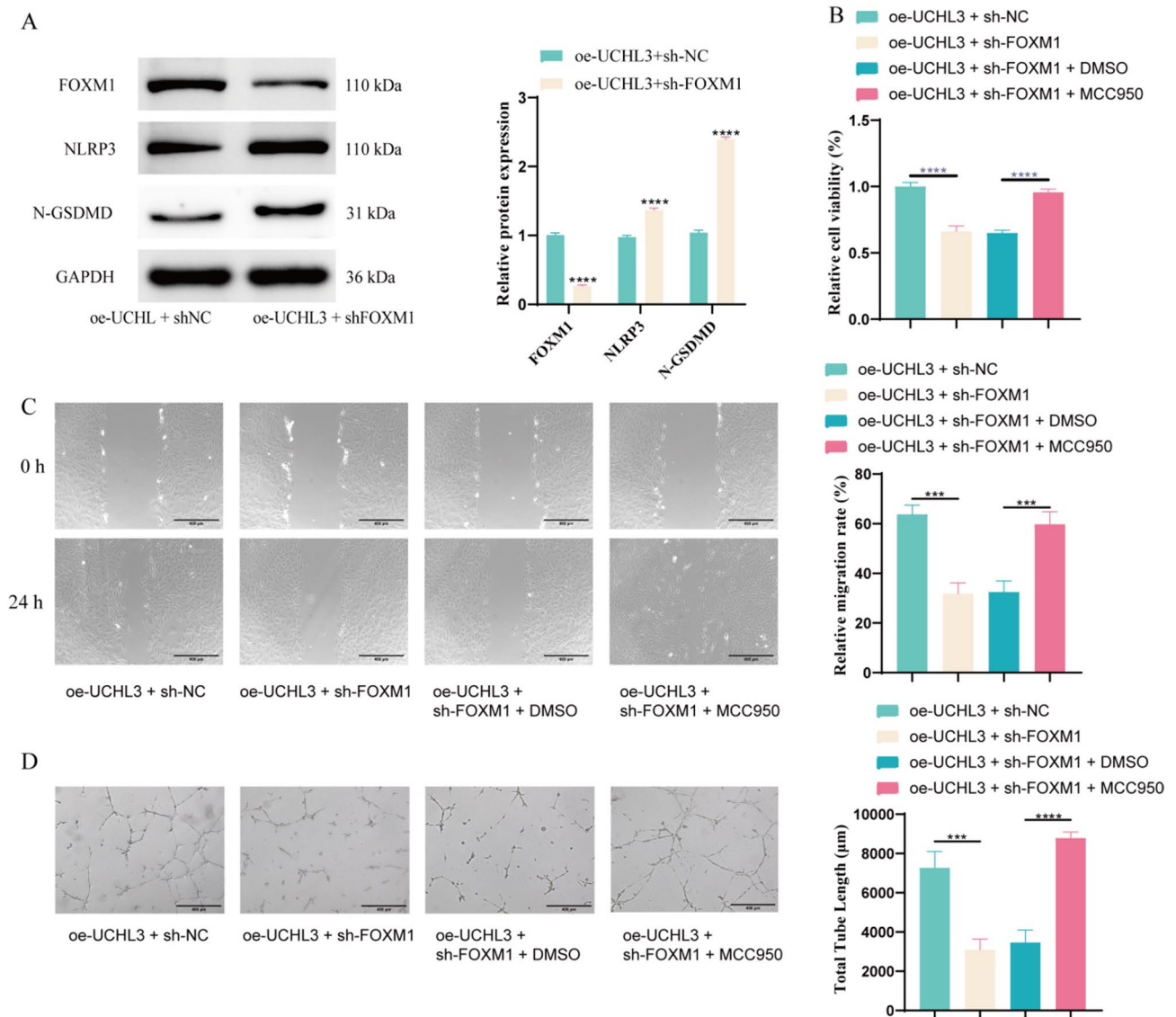


Fig. 5 Knockdown of FOXM1 leads to pyroptosis of endothelial cells and inhibits angiogenesis. **(A)** WB detection of FOXM1, NLRP3, and N-GSDMD expression in HUVECs. **(B)** CCK-8 assay measuring proliferation activity of HUVECs. **(C)** Scratch wound healing assay detecting migration ability of HUVECs. **(D)** Tube formation assay evaluating angiogenesis capacity of HUVECs. $n = 3$. The magnification of images **D** and **E** is 100 times (scale = 400 μm). *** $P < 0.001$, **** $P < 0.0001$. Three or more sets of data will be analyzed using one-way or two-way ANOVA, and Tukey's will be used for post hoc testing

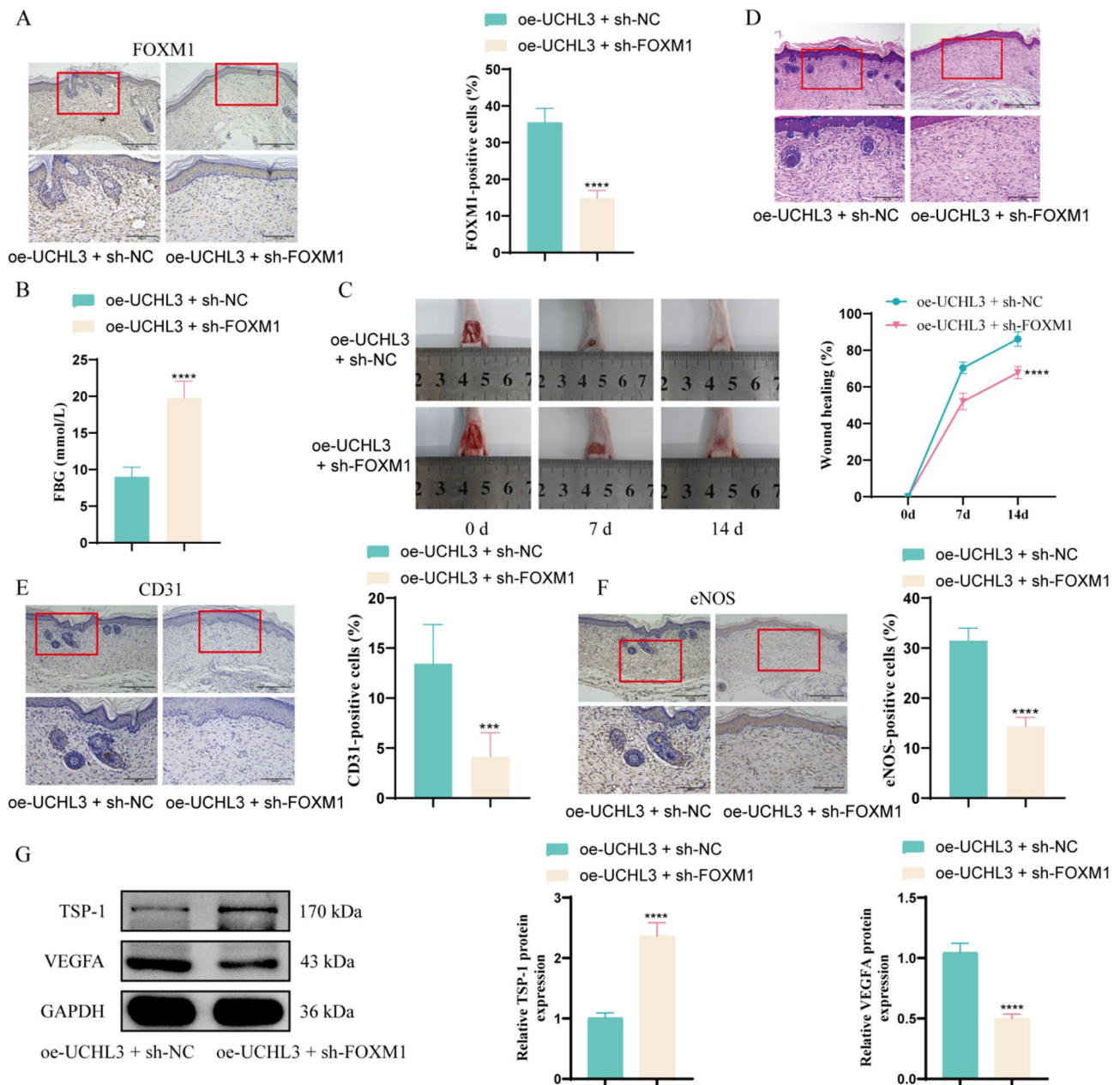


Fig. 6 UCHL3 alleviates DFU by promoting the expression of FOXM1. **(A)** Immunohistochemical detection of FOXM1 expression in rat wound tissue. **(B)** Wound healing rate assessment in rats. **(C)** Blood glucose level monitoring in rats. **(D)** HE staining analysis of wound histology and morphology. **(E)** Immunohistochemical detection of CD31 (angiogenesis marker) in wound tissue. **(F)** Immunohistochemical detection of eNOS (endothelial function marker) in wound tissue. **(G)** WB analysis of angiogenesis-related proteins (VEGF and TSP-1) in wound tissues. $n=6$. The magnification of images **A**, **D**, **E** and **F** is 100 times (scale = 400 μm) and 200 times (scale = 200 μm) respectively. ** $P < 0.01$, *** $P < 0.001$. The detection between the two groups was analyzed using t-test. Two factor analysis of variance (ANOVA) will be used for three or more sets of data, and Tukey's will be used for post hoc testing

Conclusions

In summary, this study demonstrated that UCHL3 promotes wound healing in DFU rats by binding to FOXM1 and facilitating its deubiquitination and degradation. Furthermore, UCHL3 inhibits GSDMD degradation through the FOXM1/NLRP3 inflammasome pathway, suppressing EC pyroptosis under high-glucose conditions and

promoting angiogenesis, thereby exerting a protective effect against DFU.

Acknowledgements

Not applicable.

Author contributions

Zhonghua Fu and Guanghua Guo prepared the manuscript preparation, Xincheng Liao and Zhengying Jiang designed this study. All authors reviewed the manuscript.

Funding

It is supported by National Natural Science Foundation of China (Grant No. 82160380).

Data availability

No datasets were generated or analysed during the current study.

Declarations**Ethical approval**

This experiment has been approved by the Animal Ethics Committee of Hunan Evidence-based Biotechnology Co., Ltd. (ABTZ24002). All procedures and reporting were performed according to the ARRIVE guidelines including the 3R concept.

Competing interests

The authors declare no competing interests.

Received: 1 April 2025 / Accepted: 11 May 2025

Published online: 20 May 2025

References

- Li X, Xie X, Lian W, Shi R, Han S, Zhang H, et al. Exosomes from adipose-derived stem cells overexpressing Nrf2 accelerate cutaneous wound healing by promoting vascularization in a diabetic foot ulcer rat model. *Exp Mol Med*. 2018;50:1–14.
- Ahluwalia R, Lazaro-Martinez JL, Reichert I, Maffulli N. Advances in pharmacotherapy for diabetic foot osteomyelitis. *Expert Opin Pharmacother*. 2021;22:2281–91.
- Aicale R, Cipollaro L, Esposito S, Maffulli N. An evidence based narrative review on treatment of diabetic foot osteomyelitis. *Surgeon*. 2020;18:311–20.
- Ramsey DJ, Kwan JT, Sharma A. Keeping an eye on the diabetic foot: the connection between diabetic eye disease and wound healing in the lower extremity. *World J Diabetes*. 2022;13:1035–48.
- Yan C, Chen J, Wang C, Yuan M, Kang Y, Wu Z, et al. Milk exosomes-mediated miR-31-5p delivery accelerates diabetic wound healing through promoting angiogenesis. *Drug Deliv*. 2022;29:214–28.
- Ahluwalia R, Maffulli N, Lazaro-Martinez JL, Kirketerp-Moller K, Reichert I. Diabetic foot off loading and ulcer remission: exploring surgical off-loading. *Surgeon*. 2021;19:e526–35.
- Chamberlain RC, Fleetwood K, Wild SH, Colhoun HM, Lindsay RS, Petrie JR, et al. Foot ulcer and risk of lower limb amputation or death in people with diabetes: A National Population-Based retrospective cohort study. *Diabetes Care*. 2022;45:83–91.
- Canha F, Soares R. The use of innovative targeted angiogenic therapies for ischemic diabetic foot ulcer repair: from nanomedicine and MicroRNAs toward hyperbaric oxygen therapy. *Porto Biomed J*. 2023;8:e187.
- Bitar MS. Diabetes impairs angiogenesis and induces endothelial cell senescence by up-regulating Thrombospondin-CD47-Dependent signaling. *Int J Mol Sci*. 2019;20.
- Brem H, Jacobs T, Vileikyte L, Weinberger S, Gibber M, Gill K, et al. Wound-healing protocols for diabetic foot and pressure ulcers. *Surg Technol Int*. 2003;11:85–92.
- Guo S, DiPietro LA. Factors affecting wound healing. *J Dent Res*. 2010;89:219–29.
- Kitamura H. Ubiquitin-Specific proteases (USPs) and metabolic disorders. *Int J Mol Sci*. 2023;24.
- Zhao Y, Fan S, Zhu H, Zhao Q, Fang Z, Xu D, et al. Podocyte OTUD5 alleviates diabetic kidney disease through deubiquitinating TAK1 and reducing podocyte inflammation and injury. *Nat Commun*. 2024;15:5441.
- Zhao J, Huo Q, Zhang J, Sun K, Guo J, Cheng F, et al. UCHL3 promotes hepatocellular carcinoma progression by stabilizing EEF1A1 through deubiquitination. *Biol Direct*. 2024;19:53.
- Sawaya AP, Stone RC, Brooks SR, Pastar I, Jozic I, Hasneen K, et al. Deregulated immune cell recruitment orchestrated by FOXM1 impairs human diabetic wound healing. *Nat Commun*. 2020;11:4678.
- Huang X, Zhang X, Machireddy N, Evans CE, Trewartha SD, Hu G, et al. Endothelial FoxM1 reactivates aging-impaired endothelial regeneration for vascular repair and resolution of inflammatory lung injury. *Sci Transl Med*. 2023;15:eabm5755.
- Zhen Y, Zhang H. NLRP3 inflammasome and inflammatory bowel disease. *Front Immunol*. 2019;10:276.
- Mu X, Wu X, He W, Liu Y, Wu F, Nie X. Pyroptosis and inflammasomes in diabetic wound healing. *Front Endocrinol (Lausanne)*. 2022;13:950798.
- Chen J, Liu Y, Zhang J, Yang Y, Liang H, Li T, et al. External application of human umbilical Cord-Derived mesenchymal stem cells in hyaluronic acid gel repairs foot wounds of types I and II diabetic rats through paracrine action mode. *Stem Cells Transl Med*. 2023;12:689–706.
- Lai TC, Chen YC, Cheng HH, Lee TL, Tsai JS, Lee IT, et al. Combined exposure to fine particulate matter and high glucose aggravates endothelial damage by increasing inflammation and mitophagy: the involvement of vitamin D. *Part Fibre Toxicol*. 2022;19:25.
- Lin X, Huang S, Gao S, Liu J, Tang J, Yu M. Integrin beta5 subunit regulates hyperglycemia-induced vascular endothelial cell apoptosis through FoxO1-mediated macroautophagy. *Chin Med J (Engl)*. 2024;137:565–76.
- Livak KJ, Schmittgen TD. Analysis of relative gene expression data using real-time quantitative PCR and the 2(-Delta Delta C(T)) method. *Methods*. 2001;25:402–8.
- Zhang Z, Gan Q, Han J, Tao Q, Qiu WQ, Madri JA. CD31 as a probable responding and gate-keeping protein of the blood-brain barrier and the risk of Alzheimer's disease. *J Cereb Blood Flow Metab*. 2023;43:1027–41.
- Leo F, Suvorava T, Heuser SK, Li J, LoBue A, Barbarino F, et al. Red blood cell and endothelial eNOS independently regulate circulating nitric oxide metabolites and blood pressure. *Circulation*. 2021;144:870–89.
- Sawaya AP, Stone RC, Mehdizadeh S, Pastar I, Worrell S, Balukoff NC, et al. FOXM1 network in association with TREM1 suppression regulates NET formation in diabetic foot ulcers. *EMBO Rep*. 2022;23:e54558.
- Xiao Y, Zhao C, Tai Y, Li B, Lan T, Lai E, et al. STING mediates hepatocyte pyroptosis in liver fibrosis by epigenetically activating the NLRP3 inflammasome. *Redox Biol*. 2023;62:102691.
- Li N, Zhou H, Wu H, Wu Q, Duan M, Deng W, et al. STING-IRF3 contributes to lipopolysaccharide-induced cardiac dysfunction, inflammation, apoptosis and pyroptosis by activating NLRP3. *Redox Biol*. 2019;24:101215.
- Xie J, Liu X, Wu B, Chen B, Song Q, Guan Y, et al. Bone transport induces the release of factors with multi-tissue regenerative potential for diabetic wound healing in rats and patients. *Cell Rep Med*. 2024;5:101588.
- You J, Sun J, Ma T, Yang Z, Wang X, Zhang Z, et al. Curcumin induces therapeutic angiogenesis in a diabetic mouse hindlimb ischemia model via modulating the function of endothelial progenitor cells. *Stem Cell Res Ther*. 2017;8:182.
- Armstrong DG, Boulton AJM, Bus SA. Diabetic foot ulcers and their recurrence. *N Engl J Med*. 2017;376:2367–75.
- Kerstan A, Dieter K, Niebergall-Roth E, Klingele S, Junger M, Hasslacher C, et al. Translational development of ABCB5(+) dermal mesenchymal stem cells for therapeutic induction of angiogenesis in non-healing diabetic foot ulcers. *Stem Cell Res Ther*. 2022;13:455.
- Wang Y, Li J, Huang Y, Dai X, Liu Y, Liu Z, et al. Tripartite motif-containing 28 bridges endothelial inflammation and angiogenic activity by retaining expression of TNFR-1 and -2 and VEGFR2 in endothelial cells. *FASEB J*. 2017;31:2026–36.
- Liu J, Xu J, Huang J, Gu C, Liu Q, Zhang W, et al. TRIM27 contributes to glomerular endothelial cell injury in lupus nephritis by mediating the FoxO1 signaling pathway. *Lab Invest*. 2021;101:983–97.
- He L, Yu C, Qin S, Zheng E, Liu X, Liu Y, et al. The proteasome component PSM14 drives myelomagenesis through a histone deubiquitinase activity. *Mol Cell*. 2023;83:4000–16. e6.
- Liu L, Jiang Y, Steinle JJ. TNFAIP3 is anti-inflammatory in the retinal vasculature. *Mol Vis*. 2022;28:124–9.
- Okonkwo UA, DiPietro LA. Diabetes and wound angiogenesis. *Int J Mol Sci*. 2017;18.
- Altas V, Diabetes. Endothelial dysfunction, and vascular repair: what should a diabetologist keep his eye on? *Int J Endocrinol*. 2015;2015:848272.
- Liao GB, Li XZ, Zeng S, Liu C, Yang SM, Yang L, et al. Regulation of the master regulator FOXM1 in cancer. *Cell Commun Signal*. 2018;16:57.

Publisher's note

Springer Nature remains neutral with regard to jurisdictional claims in published maps and institutional affiliations.